Generic Morphologies of Viscoelastic Dewetting Fronts

Stephan Herminghaus, Ralf Seemann, and Karin Jacobs
Applied Physics Department, University of Ulm, D-89069 Ulm, Germany
(Received 14 January 2002; published 16 July 2002)

A simple model is put forward which accounts for the occurrence of certain generic dewetting morphologies in thin liquid coatings. It demonstrates that, by taking into account the elastic properties of the coating, a morphological phase diagram may be derived which describes the observed structures of dewetting fronts. It is demonstrated that dewetting morphologies may also serve to determine nanoscale rheological properties of liquids.

DOI: 10.1103/PhysRevLett.89.056101 PACS numbers: 68.15.+e, 47.20.Ma, 47.54.+r, 68.37.Ps

When a thin liquid film beads off a solid substrate, it is eventually transformed into an ensemble of individual liquid droplets, the arrangement of which may vary strongly according to the basic mechanisms involved in the dewetting process [1–7]. In, by far, most cases, dewetting is initiated by heterogeneous nucleation of individual holes in the initial film, thus forming contact lines between the film surface and the substrate. The surface forces acting upon these contact lines give rise to moving dewetting fronts, the motion, shape, and interplay of which largely determine the final dewetting morphology.

It would be very desirable to have a theory describing the dynamics of these fronts precisely enough for extracting information on the dewetting mechanisms from the characteristics of their shape and the final droplet structure. However, the task of setting up such a theory has proven intractable thus far. Solving the Navier-Stokes equation with the moving contact line as a boundary condition is particularly complicated and entails *ad hoc* assumptions on the dynamics at the contact line [8–10]. Furthermore, it has meanwhile become clear that viscoelastic effects, which are not described by the Navier-Stokes equation, may be decisive for the evolving morphology in both advancing and receding fronts [4,11–14]. In particular, it has recently been shown [13,14] that ''elastic'' dewetting fronts may strongly differ, as to their shape and dynamics, from Newtonian ones [15]; and it has been pointed out that these findings are not accounted for by theory thus far [13]. In contrast to very recent theoretical attempts invoking rheological nonlinearities in the material properties [16,17], it will be shown in the present paper that the main features may be well accounted for by including viscoelasticity in a rather simple, linear fashion.

Let us first recall the main features to be explained, by summarizing the generic front morphologies observed thus far. Figure 1 shows dewetting fronts in liquid polystyrene films beading off silicon substrates (the fronts move from left to right). The profiles are obtained by scanning force microscopy from the rims of circular dry patches nucleated in the films [18–20]. They represent radial sections through the rims, and the radii of the holes were invariably large as compared to the width of the rims, such that the in-plane curvature of the latter can be neglected. Most commonly, one observes profiles as those shown in Fig. 1(a), with a simple decay from the crest into the undisturbed film to the right. However, when the molecular weight of the polymer is small enough [14], the shape may be qualitatively different. This is shown in Fig. 1(b), which has been obtained with polystyrene films with a molecular weight of only 2 kg/mol. A ditch is clearly visible in front of the crest, and even another small elevation to the right of the ditch is present as well, such that the front appears as a damped oscillation. The only difference between the film materials used for Figs. 1(a) and 1(b) is their molecular weight, and thus their viscoelastic properties. If the film is not too thick, the ditch may reach the substrate and pinch off the crest from the film, forming a new contact line. This happens repeatedly, such that a series of isolated crests forms in a cascade of pinch-off events, as shown in Fig. 1(c).

We shall now create a suitable mathematical description of these findings. An incompressible viscoelastic fluid may be described by the force balance [21–23],

$$\eta \Delta j = \nabla p - E \Delta \phi \,, \tag{1}$$

where η is the viscosity, j is the material current field in the film, p is the pressure, E is Young's modulus, and ϕ is a local displacement field describing the strain [23,24]. In the present treatment, we will adopt the lubrication approximation [25], thereby neglecting the normal (z) components of the current and the pressure gradient, and consider quantities averaged over the film thickness, h. The strain in the film is thereby assumed to have a uniaxial symmetry, such that ϕ may be viewed as a scalar. We then can rewrite Eq. (1) as $J(x) = -C\partial_x(p - \alpha E \partial_x \phi)$, where J is the total current in the film, and α is a numerical factor of order unity which characterizes the flow profile. The latter depends, e.g., on the friction of the film at the substrate, and it is clear that, in the case of full slippage (in which case $\alpha = 1$), the coupling of the flow to the strain will not be the same as in the absence of slip. Although the determination of α is in principle straightforward, it is rather

 0031-9007/02/89(5)/056101(4)$20.00

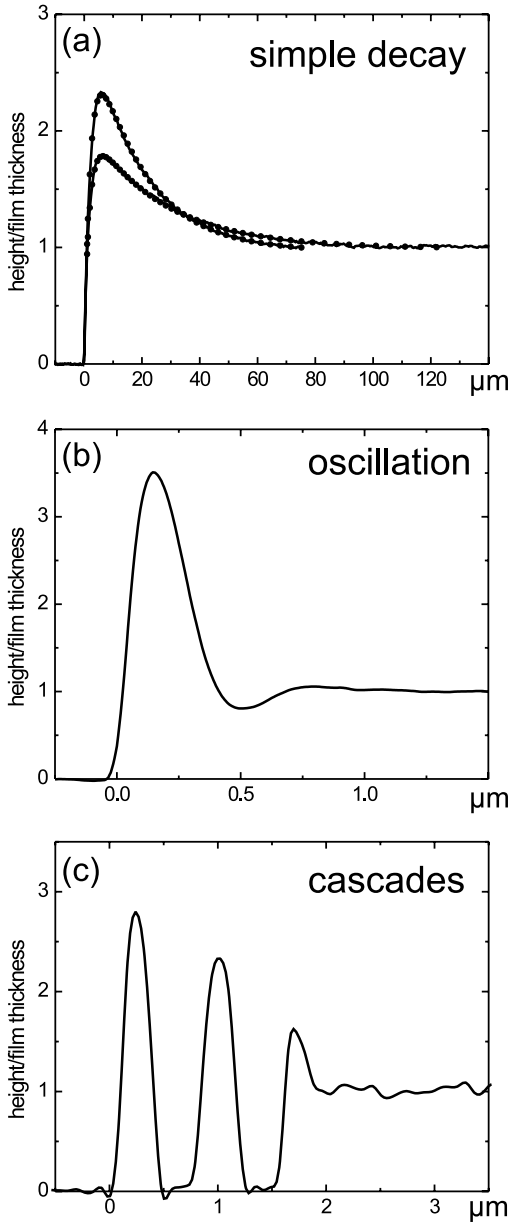

FIG. 1. Dewetting morphologies observed in various liquid polystyrene films beading off a silicon substrate. The height has been normalized with respect to the film thickness. (a) Profiles of the rims of holes nucleated in 40 nm thick films. The steep profile was obtained with a molecular weight of M_W=101 kg/mol, the flatter profile with M_W=600 kg/mol. Each profile is superimposed with a double exponential fit as a dotted line; the agreement is almost perfect (see text). (b) Profile obtained with M_W=2 kg/mol ($h = 4.9$ nm). (c) Same as (b), but with smaller film thickness ($h = 3.9$ nm).

tedious and of minor interest for the present study. Similarly, C depends upon the viscosity of the film, η, and its friction coefficient at the substrate surface, κ. If the latter is infinite (Poiseuille flow with no slip at the substrate), we have $C = h^3/3\eta$, while for $\kappa \to 0$ (plug flow), $C = h^2/\kappa$ [15,25].

Since the derivative of the displacement is the strain, $\sigma(x, t) = \partial_x \phi$, and excess pressure in the film comes about from the curvature of its surface, we have

$$J(x, t) = C\partial_x\{\gamma\partial_{xx}\zeta(x, t) + \alpha E\sigma(x, t)\}, \tag{2}$$

where γ is the surface tension, and $\zeta(x, t)$ is the vertical displacement of the film surface. We explicitly neglect long-range wetting forces acting through the film, such as van der Waals forces. In sufficiently thick films, which dewet by nucleation [19,26] (such as assumed above), these do not play a significant role.

The strain in the film may decay by internal relaxations of the material according to $\partial_t\sigma = -\omega_0\sigma$, where ω_0 is the intrinsic strain relaxation rate of the material. The coupling of the strain to the material current can thus be written as [23,24]

$$(\partial_t + \omega_0)\sigma = \partial_x J/h, \tag{3}$$

where we have neglected the nonlinear convective term $J\partial_x\phi$. This restricts our discussion to small excursions ζ, but enables a linear treatment. By combination of the above equations with the continuity equation, $\partial_t\zeta + \partial_x J = 0$, it is easy to obtain the equation of motion for σ and ζ. A precondition for elasticity to play a significant role is that $\omega_0 \ll \omega$, in which case the dispersion relation reads

$$\omega = \omega_0 + Cq^2\left(\frac{\alpha E}{h} + \gamma q^2\right), \tag{4}$$

where q is the wave number of the perturbation.

In order to determine the shape of the moving dewetting front, we now look for traveling-wave solutions of the form $\zeta(x, t) = \zeta(x - vt)$, where v is the velocity of the dewetting front. We remain in Fourier space; i.e., we decompose the front profile into modes $\zeta_q \propto \exp(iqx - \omega t)$. Writing $Q := iqh$, it follows that $\omega = Qv/h$, and from Eq. (4) we then get

$$Q^4 - \frac{\alpha Eh}{\gamma}Q^2 - \frac{vh^3}{\gamma C}Q + \frac{\omega_0 h^4}{\gamma C} = 0. \tag{5}$$

As it will become clear below, the term $\omega_0 h^4/\gamma C$ is rather small. If we neglect it for the moment, we get the cubic equation,

$$Q^3 - \tilde{E}Q - \tilde{v} = 0, \tag{6}$$

where we have introduced the dimensionless quantities $\tilde{v} := \frac{vh^3}{C\gamma}$ and $\tilde{E} := \frac{\alpha Eh}{\gamma}$. This can be easily solved, and the solutions of the quartic Eq. (5) turn out to deviate significantly from those of the cubic Eq. (6) only for parameters which are not relevant in most experimental situations. We will thus primarily discuss Eq. (6), and refer to Eq. (5) only occasionally, where appropriate.

If viscoelastic effects are absent, i.e., $E = 0$, we have $Q = \sqrt[3]{\tilde{v}}$. We are interested only in modes with $\Re(Q) < 0$ [27], which are $Q = -\frac{1}{2}\sqrt[3]{\tilde{v}}(1 \pm i\sqrt{3})$. The shape of the real surface of the leading front thus exhibits not only a

ditch, but a damped oscillation [14,28]. For Newtonian liquids, it can be seen from numerical solutions of the moving front problem that this result does *not* depend upon the friction of the film at the substrate (slippage) [11,12]. This fact is well accounted for by our model, since for $E = 0$ the ratio $\Im(Q)/\Re(Q)$ depends neither on α nor on C, which are both affected by slippage.

A profile exhibiting a damped oscillation is shown in Fig. 1(b), and it is obtained only for small molecular weight indeed, where elastic effects are particularly small. The real and imaginary part of Q can be determined from the profile, and, in the case of the one displayed in Fig. 1(b), it turns out that the oscillation decays faster than expected for a Newtonian fluid [14]. Since the complex roots of Eq. (6) satisfy the simple relation,

$$3\Re(Q)^2 - \Im(Q)^2 = \tilde{E}, \tag{7}$$

the elasticity of the film can be inferred from the measurements, and we get $\alpha E = \gamma\tilde{E}/h = 8.7$ kPa. We point out that this is a noninvasive method of determining rheological properties of complex fluids on a submicron scale.

As the height of the crest, H, increases while more material is accumulated, the amplitude of the oscillation increases, and so does the depth of the ditch [14]. When the latter reaches the substrate, the crest is pinched off and a cascade is formed as shown in Fig. 1(c). However, this works only as long as the width, W, of the crest is less than half the wavelength of the damped oscillation. As H increases, so does W [19,25], with the ratio $H/W =: G(\Theta)$ being only a function of the dynamic contact angle at the substrate, Θ [19]. For a cylindrical rim [25], we have simply $G(\Theta) = (1 - \cos\Theta)/2\sin\Theta$. For more asymmetric shapes, the form of G is different, but similar as to the overall behavior and the order of magnitude. If W is larger than $W_c = \lambda/2 = \pi/\Im(Q)$, the depth of the ditch is rather determined by the contact angle of the rim at the leading edge. Consequently, it will reach a final maximum depth [14], and a dry spot forms only if this depth exceeds the film thickness. The condition for the front to cascade is readily seen to be

$$\pi G(\Theta) > |\,\Im(Q)\,| \exp\left(\pi \frac{|\,\Re(Q)\,|}{|\,\Im(Q)\,|}\right). \tag{8}$$

If the film thickness decreases, so does the right-hand side of Eq. (8) (h cancels out in the exponential), such that a cascade is expected at sufficiently small h.

Equation (8) can be used to determine the boundary line for the appearance of cascade structures in the $(\tilde{v}, \tilde{E})$ plane. In Fig. 2(a), this is indicated by the lower curve for the case $G(\Theta) = \pi^{-1}$. For different values of G, the maximum of the boundary line, indicated by the dot in the figure, is quite accurately described by $\tilde{E} = 0.06G^2$. It is clear that, although this line gives an idea of the phase boundary, it cannot be really accurate, since cascading necessarily leads far out of the linear regime, to which we restrict our discussion here. For very thin films, where van der Waals forces play a role, the cascade region will slightly extend or shrink, depending on the sign of the Hamaker constant. These aspects will be left to a forthcoming study.

Let us now turn to the influence of stronger elastic effects. It is interesting to investigate at which system parameters the damped oscillation, as shown in Fig. 1(b), vanishes. These are given by the zero of the discriminant of the cubic Eq. (6), which is

$$D = \left(\frac{\tilde{v}}{2}\right)^2 - \left(\frac{\tilde{E}}{3}\right)^3. \tag{9}$$

The critical modulus above which there is no oscillation is thus given by $\tilde{E} = 3(\frac{\tilde{v}}{2})^{2/3}$. This may be viewed as another morphological "phase boundary" in the $(\tilde{E}, \tilde{v})$ plane, and is shown in Fig. 2(a) as the upper solid curve. The exact boundary, according to Eq. (5), deviates noticeably only for very small values of $\tilde{E}$ and $\tilde{v}$. To quantify this deviation, it is useful to introduce the dimensionless parameter $\Omega := \omega_0 h/v$, which represents the importance of intrinsic relaxation in the material with respect to the shear flow exerted by the dewetting process itself. In Fig. 2(b), the

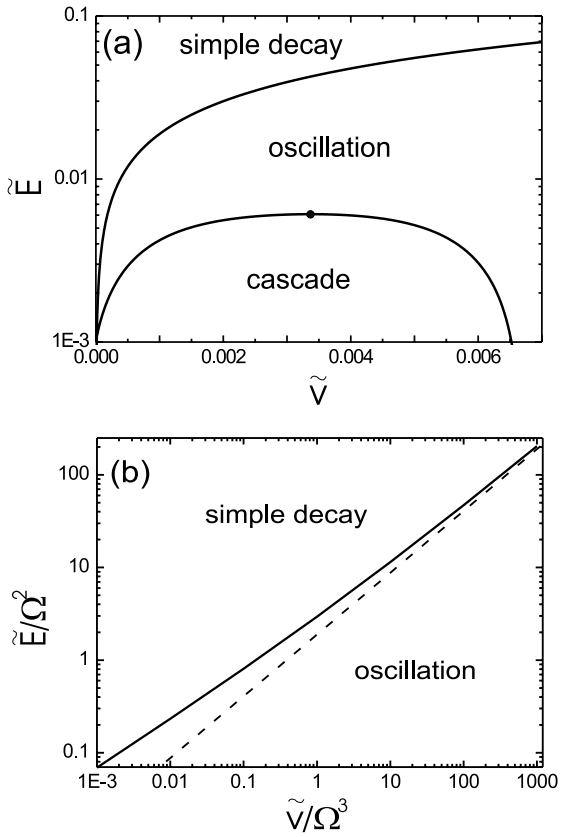

FIG. 2. (a) Morphological phase diagram for viscoelastic dewetting fronts in the $(\tilde{E}, \tilde{v})$ plane, according to Eq. (6). (b) Deviation of the phase boundary according to Eq. (5) (solid curve) from the approximation given by Eq. (6) (dashed line).

"exact" phase boundary, which was determined by solving Eq. (5) numerically, is shown as the solid curve, along with the approximation obtained from the cubic equation (dashed line). For $\Omega \to 0$, the solid curve approaches the dashed line asymptotically. The diagram presented in Fig. 2(a), which corresponds to $\Omega = 0$, shall thus be considered quite reliable within the range displayed if $\Omega < 0.1$ (in the experiments in Ref. [13], $\Omega \approx 10^{-5}$).

The two complex conjugate roots, which give rise to the oscillations for $D > 0$, merge into a degenerate real root at a critical elastic modulus ($D = 0$). As the latter increases further, they bifurcate again into two real roots, Q_{long} and Q_{short}. In fact, elastic fronts can be well fitted by a superposition of two exponentials, as shown in Fig. 1(a) by the dotted curves. The model predicts the ratio $Q_{\text{short}}/Q_{\text{long}}$ to increase with $\tilde{E}$, and thus the front to become more and more asymmetric, in accordance with observation [4,13,14]. We can again determine $\tilde{E}$ from the front profile via the relation

$$\frac{Q_{\text{long}}}{Q_{\text{short}}} = \frac{\sin\{\frac{\pi}{6} - \frac{1}{3}\arccos B\}}{\sin\{\frac{\pi}{6} + \frac{1}{3}\arccos B\}}, \tag{10}$$

with $B := \frac{3}{2}\sqrt{3}\tilde{v}\tilde{E}^{-3/2}$, once the constant C is known for the system.

The long-range shape of the front is determined by the smaller root, Q_{long}, which asymptotically approaches the simple law $Q = -\tilde{v}/\tilde{E}$. Since our model predicts Q_{short} to scale as $\sqrt{\tilde{E}}$ for sufficiently large $\tilde{E}$, we have $Q_{\text{long}} \propto Q_{\text{short}}^{-2}$ if all other parameters in the system are kept constant. In fact, for the two curves shown in Fig. 1(a), the ratio of the Q_{long} is 1.40 ± 0.07, while the ratio of the Q_{short}^{-2} is 1.34 ± 0.13. This is clear agreement.

Finally, we note that, for large molecular weight, the width of the front is found experimentally to remain constant as it moves over the substrate [13]. This is in contrast to what one observes with Newtonian fronts [15], but is precisely what our model predicts: a well-defined decay length, independent of the distance traveled.

We thus have put forward a tractable, linear model which describes, on the basis of viscoelasticity, the generic morphologies of liquid dewetting fronts observed thus far. It correctly accounts for the impact of the fluid properties upon their occurrence and structure. It is thereby capable of extracting information on the submicron scale rheological properties of the liquid film from the observed profiles. This may be rendered quantitative by determining the numerical constant α, which we leave to further work.

The authors are indebted to Klaus Mecke and Ralf Blossey for many fruitful discussion. We also thank Günter Reiter for stimulating remarks, and for making accessible to us some data from Ref. [13]. Funding from the Deutsche Forschungsgemeinschaft within the Priority Program 1052 "Wetting and Structure Formation at Interfaces" is gratefully acknowledged.

[1] D. J. Srolovitz and S. A. Safran, J. Appl. Phys. **60**, 247 (1986).
[2] C. Redon, F. Brochard-Wyart, and F. Rondelez, Phys. Rev. Lett. **66**, 715 (1991).
[3] G. Reiter, Phys. Rev. Lett. **68**, 75 (1992).
[4] K. Jacobs, Ph.D. thesis, Konstanz, 1996; ISBN 3-930803-10-0.
[5] P. Lambooy, K. C. Phelan, O. Haugg, and G. Krausch, Phys. Rev. Lett. **76**, 1110 (1996).
[6] T. G. Stange, D. F. Evans, and W. A. Hendrickson, Langmuir **13**, 4459 (1997).
[7] S. Herminghaus *et al.*, Science **282**, 916 (1998).
[8] J. Moriarty, L. Schwartz, and E. Tuck, Phys. Fluids A **3**, 733 (1991).
[9] H. Greenspan, J. Fluid Mech. **84**, 125 (1978).
[10] S. Troian, E. Herbolzheimer, S. Safran, and J. F. Joanny, Europhys. Lett. **10**, 25 (1989).
[11] M. Spaid and G. Homsy, J. Non-Newtonian Fluid Mech. **55**, 249 (1994).
[12] M. A. Spaid and G. M. Homsy, Phys. Fluids **8**, 460 (1996).
[13] G. Reiter, Phys. Rev. Lett. **87**, 186101 (2001).
[14] R. Seemann, S. Herminghaus, and K. Jacobs, Phys. Rev. Lett. **87**, 196101 (2001).
[15] K. Jacobs, R. Seemann, G. Schatz, and S. Herminghaus, Langmuir **14**, 4961 (1998).
[16] F. Saulnier, E. Raphael, and P.-G. De Gennes, Phys. Rev. Lett. **88**, 196101 (2002).
[17] V. Shenoy and A. Sharma, arXiv.org (2002), cond-mat/0202160.
[18] G. Reiter, P. Auroy, and L. Auvray, Macromolecules **29**, 2150 (1996).
[19] K. Jacobs, S. Herminghaus, and K. Mecke, Langmuir **14**, 965 (1998).
[20] D. Podzimek *et al.*, cond-mat/0105065 (2001).
[21] L. D. Landau and E. M. Lifshitz, *Theory of Elasticity* (Butterworth, London, 1995), Vol. VII.
[22] L. Landau and E. M. Lifshitz, *Hydrodynamics* (Butterworth, London, 1995), Vol. VI.
[23] S. Herminghaus, K. Jacobs, and R. Seemann, Eur. Phys. J. E **5**, 531 (2001).
[24] S. Herminghaus, Eur. Phys. J. E (to be published).
[25] F. Brochard-Wyart, P.-G. de Gennes, H. Hervert, and C. Redon, Langmuir **10**, 1566 (1994).
[26] R. Seemann, S. Herminghaus, and K. Jacobs, Phys. Rev. Lett. **86**, 5534 (2001).
[27] $\Re(\cdot)$ and $\Im(\cdot)$ denote the real and the imaginary parts of their argument, respectively.
[28] The same result is obtained for surface diffusion kinetics [D. J. Srolovitz and S. A. Safran, J. Appl. Phys. **60**, 255 (1986)].